21, rue d'Artois, F-75008 PARIS
http : //www.cigre.org

CIGRE US National Committee
2022 Grid of the Future Symposium

Virtual Synchronous Controller Based SMES/Battery Energy Storage System

M.M. BADRELDIEN, B.K. JOHNSON
University of Idaho
USA

SUMMARY

Utilities have embraced renewable energy resources, especially wind and photovoltaic power plants for generating electric power. However, these resources aren't dispatchable nor are they stable resources since their output power experiences frequent power fluctuations. Furthermore, these resources when connected via grid following power converters have low inertia and they tend to reduce the total system inertia. Hence, the power system may be vulnerable to stability problems. To overcome these issues, converters connected to energy storage systems are integrated with these renewable energy resources, controlled to provide virtual inertia and emulate the inertial response features of the conventional synchronous generator to improve the system's stability. A hybrid energy storage system built around a battery combined with a superconducting magnetic energy storage system is proposed to provide this virtual inertia.

The superconducting magnetic energy storage system is a high-power density system with fast response to accomodate high-frequency power fluctuations and emulate the inertial response of the traditional synchronous generator. On the other hand, the battery provides high energy and deals with low-frequency power fluctuations. This hybrid system reduces the stress on the battery due to supplying the transient and high charging and discharging currents, and so increases the battery lifetime.

This paper describes general features offered by the hybrid energy storage system and its controller. Also, the effects of inertia and damping constants emulation on the system response are described. Furthermore, the effects providing emulated inertia and damping on the power rating of the two converters and the energy ratings of the two energy storage systems are described. The system simulation is verified using an electromagnetic transient simulation program.

KEYWORDS

Superconducting magnetic energy storage, battery energy storage system, virtual synchronous generator, inertia emulation

Badr6124@vandals.uidaho.edu

1.INTRODUCTION

The desire to reduce the carbon footprint caused by fossil-fuelled power plants has increased the adoption of renewable energy resources (RERs) and distributed generating units (DGUs) in particular photovoltaic (PV) plants in the power system network. Furthermore, the topology and architecture of the power system have changed from a system with large conventional, centralized, and dispatchable power generators to one with non-conventional distributed generating resources.

The power output from these RERs and DGUs depends on uncontrolled environmental factors. Their power output fluctuates according to the availability of the resources which are intermittent and uncontrollable, and sometimes they may fail to meet the load demand. So the reliability of generating resources to supply the available loads continuously is reduced. Also, increasing their penetration in the power system may cause stability problems. Such issues have become major hurdles to the widespread of RERs in power systems especially small systems such as microgrids.

The most common problem is the reduction of the intrinsic kinetic energy (rotor inertia) and damping property that results from the mechanical friction and electrical losses in stator, field, and damper windings of the conventional synchronous generators (CSGs). Hence, there is a reduction in the total system inertia. RERs such as wind power plants have a low inertia and PV systems don't have any rotating kinetic energy. This system inertia reduction makes the system vulnerable to stability problems. The system may lose synchronism in case of disturbances such as a sudden change in loads or power generations or fault occurrences [1].

One of the proposed solutions to solve these problems is integrating energy storage systems (ESSs) with RERs. ESSs can store the energy at off-peak periods and supply the required load at peak periods, so they achieve the power balance between the supply and demand. Furthermore, they can be included in a system for emulating the conventional synchronous generator to compensate for the lack of rotating inertia to address the transient changes. This methodology is known as a virtual synchronous generator (VSG) [2], [3]. These ESSs help to provide virtual inertia to improve the system stability against different disturbances. Furthermore, the continuous research and developments in ESSs technologies improved the cost effectiveness of ESSs as viable solutions for power system applications. The authors of [4], [5] described how they can be used for power balancing, smoothing power flow, fluctuation suppression, black start, and voltage and frequency control.

One of the popular types of ESSs is the battery energy storage system (BESS). Battery systems have been used for a long time in power system applications. They have been used in storage energy applications. Batteries have many advantages such as high energy density, high efficiency, long life, and low self-discharge. Then, BESSs can be used in power system applications such as power quality enhancement, energy management, and smoothing the long-term power fluctuations in microgrids. The authors of [6] described the usage of batteries in power system applications in detail.

On the contrary, batteries have some disadvantages that make them unable to achieve all the system requirements. Due to the chemical kinetic involvement, batteries have a low response time, a limited voltage and current rating, and so low power capacity. Hence, BESSs can't respond rapidly to the different transients in power systems. Furthermore, they have a poor life cycle, so the number of lifetime charging and discharging cycles is limited. Moreover, the deep frequent charging and discharging processes shorten the battery lifetime, since the heat produced from the chemical reaction in these operations reduces their lifetime. Also, some environmental hazards may be caused by batteries during their charge and discharge processes and disposal of their hazard materials.

To address the limitations of the batteries and improve the operational performance of the power system, a hybrid energy storage system (HESS) is proposed. The authors of [7], [8] described the different types of ESSs, their contributions to HESS, and their effect on improving power system operation. HESS can be implemented to provide high energy and power capabilities and rapid response time. Hence, they can address the different transient disturbances, smooth the power flow, and improve the system's stability and operation. Then, the HESS reduces battery cycling and the stresses due to large charging and discharging currents at different transient periods. So the battery lifetime is being improved.

There are various types of ESSs that can be integrated with the batteries to form HESS. The most common energy storage types are pumped storage hydroelectric systems, flywheels, supercapacitors, and superconducting magnetic energy storage (SMES). The authors of [8] summarized these ESSs and their usage in microgrids in detail.

The SMES can overcome the batteries disadvantages and support the power system operation. Moreover, it can address the short-term transient power [9]. Then, in this paper, SMES will be used in conjunction with the battery system to form a HESS for improving the operation of the system.

In this paper, the importance of the SMES system and its advantages are described. In addition,, modeling and control of the dc-dc SMES converter are presented. Moreover, the battery control system is modeled and described. Hereafter, the simulation of the proposed control methodologies is carried out using an electromagnetic transient simulation program.

The rest of this paper is arranged as follows. Section 2 describes the system layout. In Section 3, the dc-ac converter controller is described. In Section 4, the SMES system and its controller are presented. Section 5 describes the BESS and its controller. Hereafter, simulation of the proposed system is introduced in section 6. Finally, in Section 7, some relevant conclusions are drawn.

2. SYSTEM LAYOUT

The proposed system layout is shown in Fig. 1. In this system, a VSG-based controller is exploited to control the PV system which is connected with a HESS. The main source of electrical energy in this system is the PV array. It generates electrical power at a low voltage and is stepped up using a dc-dc boost converter to match the dc-link voltage. Furthermore, it maximizes the energy extracted from the PV array by using a maximum power point tracking scheme. A detailed description of the PV array and its boost converted are described in [10]-[12].

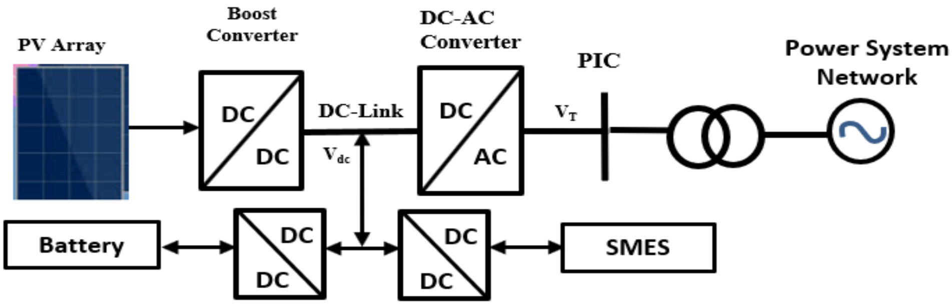

Fig. 1. General layout of the proposed system

The dc-ac converter and the HESS are controlled to emulate the conventional synchronous generator features such as damping and inertia constants. The operation of the converter depends on the dc-link configuration where the power fluctuation due to the different disturbances is compensated from the dc-link and then from the storage systems. HESS is composed of SMES and battery, and they are connected to a common dc-link.

The SMES responds to high frequency and short-time disturbances, it can support the system with high current and high power in a short time. It interacts with the variations of the dc-link voltage magnitude. In case of disturbance that causes the system output power to exceed the PV generated power, the dc-link voltage decreases, and the SMES discharges to keep the dc-link voltage constant. Contrarily, if the disturbance causes the dc-link voltage to increase, the SMES charges to return the dc-link voltage back to the nominal range values.

On the other hand, the battery addresses the low-frequency fluctuation. If the generated power doesn't match the demand power, the battery compensates for the difference to stabilize the system. The battery can handle cases that require high energy capacities.

Hence, the HESS can support the system at different disturbances, improve the system's stability and operation, and provide both high power and energy capabilities.

DC-AC converter delivers power from the dc-link to the grid which is simulated by a voltage source in this paper. The model and the control system of the converter are implemented in a direct and quadrature (dq) reference frame. It is described in detail in [13]-[14]. In the following subsections, a description of the dc-ac converter controller, the HESS and its controllers will be presented.

3. DC-AC CONVERTER CONTROLLER

The dc-ac converter emulates the CSG features, damping and inertia constants. Its controllers are described in the following subsections.

A. Outer Loop: Inertial Emulation

The swing equation of the conventional SG that can be derived from Newton's Law of Motion for rotating objects can be written as [15]:

$$T_m - T_e - D(\omega - \omega_g) = J(d\omega/dt) \quad (1)$$

where T_m is the mechanical driving torque from the prime mover, T_e is the electromagnetic torque that affects the rotor. D is the damping coefficient accounting for the damping torque associated with the damper windings, ω is the rotational speed of the machine, and ω_g is the grid frequency, J is the rotor inertia.

It is more common to write the swing equation expressed in equation (1) in terms of power instead of torque, by multiplying the equation (1) by frequency ω. In case of a little oscillation around the synchronous speed, the equation representing the power balance which is represented in the Laplace domain is expressed as [15]:

$$P_m - P_e - K_d(\omega - \omega_g) \approx J \, \omega_g S \; \omega \qquad (2)$$

where P_m is the emulated mechanical input power, P_e is the electrical output power, and K_d is the damping constant associated with the constant D. Equation (2) can be expressed in per unit as:

$$P_m - P_e - K_d(\omega_{pu} - \omega g_{pu}) \approx T_a \; \omega_{pu} S \qquad (3)$$

where the time constant $T_a = 2H$, H is the per unit inertia constant for the stored kinetic energy in the rotor at rated speed divided by the chosen MVA base. The block diagram describing the swing equation is shown in Fig. 2. The output power P_o should follow the reference power P_{ref} set to the converter. Also, the output active power is associated with the VSG emulated torque and angular speed of the rotor ω_{VSG}. The virtual rotor angle δ_{VSG} generated from Fig. 2 emulates the phase angle of the voltage induced by VSG and it is used in the Park's transformation and in the inner loops on the converter controllers.

B. Outer Loop: Voltage Controller

The VSG voltage magnitude is controlled by a decoupled voltage or reactive power control loop. Fig. 3 describes the voltage control outer loop that generates the voltage control signals. The reference voltage signal (V_{d_ref}) is aligned to coincide with the direct axis of the converter voltage reference frame and the quadrature axis voltage is set to zero. Controlling the terminal voltage (V_T) to follow the reference grid voltage ($V_{ac\text{-}ref}$), enables the converter to operate on both grid connected and isolated modes of operations.

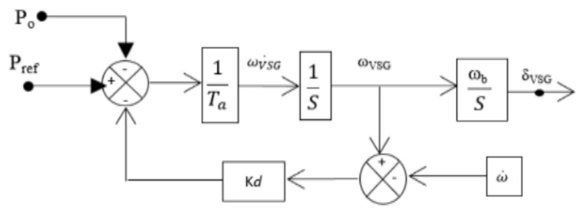

Fig. 2. Virtual inertia emulation

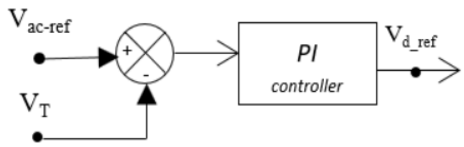

Fig. 3. Voltage controller

C. Cascaded Inner Voltage and Current Control Loops

The inner control loops consist of two cascaded loops. The first loop is the voltage control loop that generates the reference current signals (I_{d_ref} , I_{q_ref}) to the second current loop. The second current control part controls the direct and quadrature current components (I_d, I_q) to follow its reference values. The inner cascaded loops are shown in Fig. 4. The system is modeled in a synchronously rotating dq reference frame and proportional integral (PI) controllers are used to control the system. The inner loop generates the modulation indexes (M_d, M_q) that used to drive the switches.

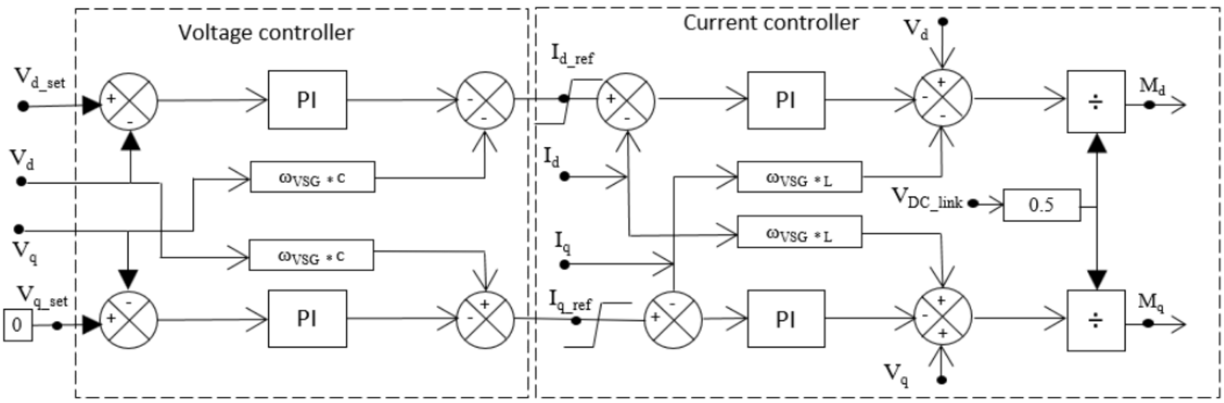

Fig. 4. Cascaded voltage and current control loops

4.SMES SYSTEM AND CONTROLLER

Superconductivity was discovered in 1911, but the research and development of its application in power systems started in the 1970s. SMES stores the electric energy in a magnetic field generated by the current flowing through superconducting wires configured in coils. SMES has many advantages that make it viable in power system applications. It has a high power density, low-self discharge rate, large number of charge and discharge cycles, high efficiency, and ease of controllability. Moreover, it can handle a high peak current and power, so it is a viable solution to handle the short-term power oscillations and improve power system operations [16]. SMES system can be used for controlling both the active and reactive power and so the voltage and the frequency of the system.
Fig. 5 shows the schematic diagram of the SMES system. It consists of three main parts; superconducting coil, cryostat refrigeration system, and power conditioning unit (PCU). The superconducting coil is made of superconducting material which may be a low-temperature superconducting material (LTS) that works at ≈ 5 k or high-temperature superconducting material (HTS) that works at ≈ 70k. The coil is immersed in a dewar consisting of a vacuum vessel and liquid vessel with a coolant liquid such as Helium or Nitrogen to maintain the coil temperature below the superconducting critical temperature.
The cryostat or refrigeration system reduces the temperature of the coil to keep it in its superconducting state during SMES operations.
The power conditioning unit addresses power transfer between the coil and the power system. The VSC-based SMES system is used in this work. It consists of a dc-dc chopper and dc-ac converter. It controls the dc-link voltage by controlling the power transfer between the coil and the dc-link.
Fig. 6 shows the dc-dc chopper that connects the SMES coil to the dc-link. The energy stored in the SMES coil and the available power are proportional to the current flowing it and can be expressed as:

$$E_{stored} = 0.5\, LI^2_{coil} \quad (4)$$

$$P_{SMES}=(dE/dt)=V_{dc} * I_{coil} \quad (5)$$

where L is the coil inductance, I_{coil} is the SMES coil current, and V_{dc} is the dc-link voltage. The power flow is controlled to keep the dc-link voltage magnitude within the normal operating range.
In the charging process, both the switches S_1 and S_2 are turned on, and the coil current increases. On the contrary, when both switches are turned off, the SMES turns to the discharge state, and it delivers the power to the dc-link. When switch S_1 is turned off and the switch S_2 is turned on, the SMES coil is no longer charged nor discharged, and this is the standby mode.
The dc-chopper circuit allows the SMES coil to control the dc-link voltage variation within milliseconds such that it may change from charge to discharge states at this time. This high-speed response allows the SMES system to provide a spinning reverse to enhance the system's operation and stability.
Although the SMES system is a competitive ESS in power system application to improve stability, it has some disadvantages such as high cost and coil sensitivity to temperature variations. However the SMES system has a high cost today, the continuous research and developments in the SMES systems is projected to finally drive its cost down.

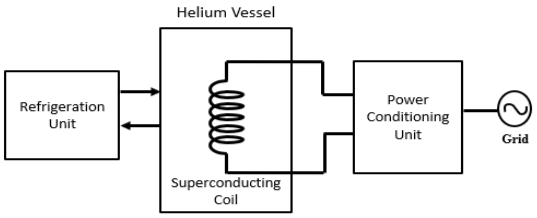

Fig. 5. Schematic diagram of a SMES system

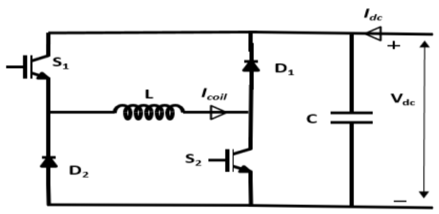

Fig. 6. DC-DC chopper of the SMES coil

5.BESS AND CONTROLLER

Batteries are widely exploited in power system applications because of their ability to supply high energy. Moreover, they are the most cost-effective energy storage system. The battery system consists of several parallel and series combinations of battery modules to produce the desired electrical requirements. It is considered the low-cost storage option in power system applications. Batteries require an interface circuit to connect them to the dc-link. Fig. 7 describes the circuit of the bi-directional buck-boost converter that controls the charging and discharging processes of the batteries. It is described in details in [12].
The equivalent circuit model is used for modeling the battery. The battery is represented by a controlled voltage source which is connected in series with a resistance representing the internal resistance of the battery as shown

in Fig. 8. The equations representing the battery voltage during charging and discharging processes are expressed in equations (6) and (7) [12].

$$E=E_o - K(Q/(Q - it))+A.e^{(-B.\int idt)} \quad (4)$$

$$V_b = E - R_i * i \quad (5)$$

where E is no load voltage source controller (V), E_o is a battery constant voltage (V), Q is the battery's capacity (Ah), K is polarization voltage constant (V), the integral $\int i\, dt$ represents the actual battery charge (Ah), B is the exponential constant inverse capacity $(Ah)^{-1}$, A is exponential voltage zone amplitude (V), R_i is the battery internal resistance (Ω), V_b is the battery terminal voltage (V) and i is the battery current (A). A detailed explanation of the battery model is described in [17].

Controlling the state of charge (SoC) within certain limits is important to increase the battery lifetime. Battery SoC increases with charging and decreases with the discharging process as per energy conservation law. The controller limits the SoC to be within a range of 20-85 %.

Since the battery has a high energy density, it handles the low power fluctuations, charges, and discharge slowly, and lasts a long time to respond to the system. Then, it meets the steady demand of the system which increases the battery lifetime.

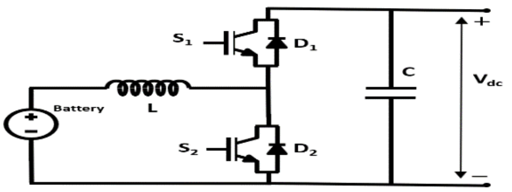

Fig. 7. Bi-directional buck-boost converter

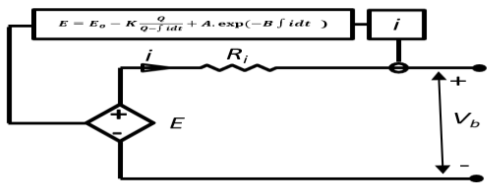

Fig. 8. Equivalent circuit of the battery

6. SIMULATION RESULTS

To verify the proposed control structure, the system that is shown in Fig. 1 is implemented and modeled in an electromagnetic transients program. The simulation is carried out at different scenarios for different conditions to clarify the operation of the HESS controller and how the converter emulates the CSG inertial features. Moreover, it describes how the inertia and damping constants affect the operation of the system and the rating of both the converter and ESS power and energy. The first scenario describes the VSG at grid frequency change and how it emulates the inertial features of the CSG when the grid frequency changes. The simulation is done at different values of damping and inertia time constants. Fig. 9 describes the drop in frequency from 60 Hz to 59.4 Hz due to an event on the external microgrid.

The converter output power changes in response to the grid frequency change as shown in Fig. 10. The power profile depends on the damping constant value, such that when the damping constant increases the output power has less magnitude and oscillations and reaches its steady state sooner. The power and the energy generated in response to the frequency change are supplied from the SMES system. The SMES is charged at 2.35 MJ at the start of the simulation. As shown in Fig. 11 and Fig. 12, when the damping constant increases, the peak power and energy required from the SMES system is decreased. Moreover, the SMES can supply 0.5pu in a very short time; less than 0.2 sec which is faster than the battery response and protect the battery from this high discharge or charge rate.

It is shown that the damping constant affects the design and rating of both the converter and the SMES system. Fig. 13 describes the change in the maximum converter output power values with respect to the damping constant and how the converter power is affected by the damping constant. It can be seen that the converter power is reduced when the damping constant increases. Fig. 14 and Fig. 15 describe the supplied SMES power and energy with respect to the damping constant, and how the size of the SMES system is reduced with increasing the damping constant. Then the SMES energy and power design and rating should be based on the emulated damping constants. The simulation results show that when the damping constant increases, the maximum converter output power decreases, and hence, the power required from the HESS decreases.

The previous simulation case is repeated at different inertia time constants. This case describes how the inertia time constant change affects the converter output power and the SMES system performances. Fig 16 describes the converter output power. It is seen that when the inertia time constant increases, the converter supplies more inertial power. This power is supplied by the SMES system. Fig. 17 and Fig. 18 describe the SMES power and energy at different inertia time constants. It can be shown that by increasing the inertia time constant, the SMES power and energy increase.

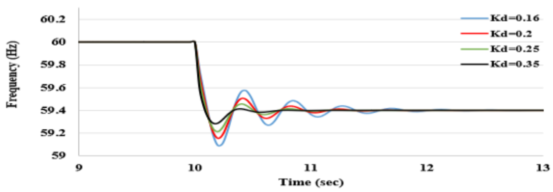

Fig. 9. Response to a microgrid frequency drop at different damping constants

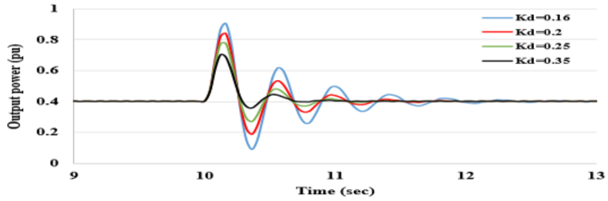

Fig. 10. Converter output power at different damping constants in response to a microgrid frequency drop

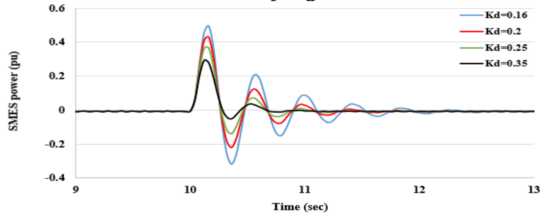

Fig. 11. SMES instantaneous power in response to a microgrid frequency drop

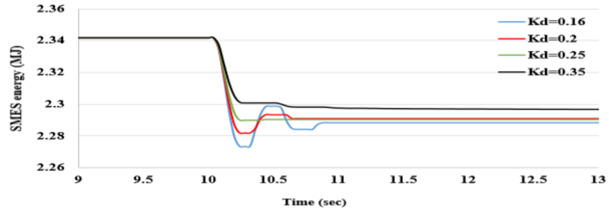

Fig. 12. SMES energy at different damping constant in response to a microgrid frequency drop

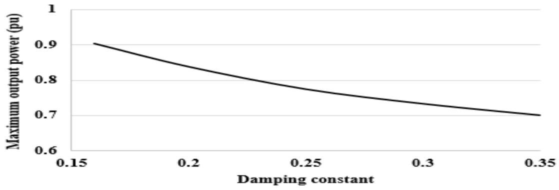

Fig. 13. Maximum output power versus damping constant in response to a microgrid frequency drop

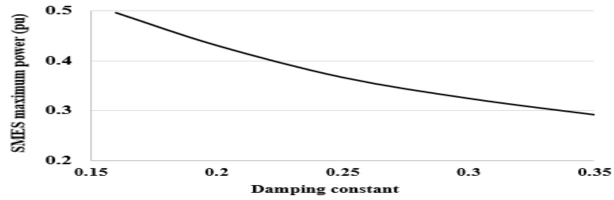

Fig. 14. SMES maximum power versus damping constant in response to a microgrid frequency drop

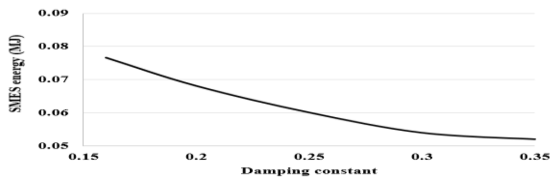

Fig. 15. SMES energy versus damping constant in response to a microgrid frequency drop

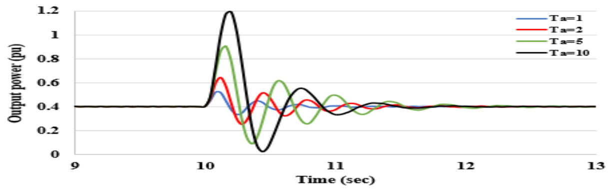

Fig. 16. Output power at different inertia constants in response to a microgrid frequency drop

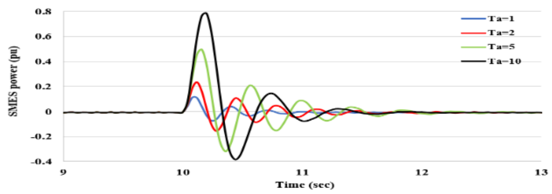

Fig. 17. SMES power at different inertia constants in response to a microgrid frequency drop

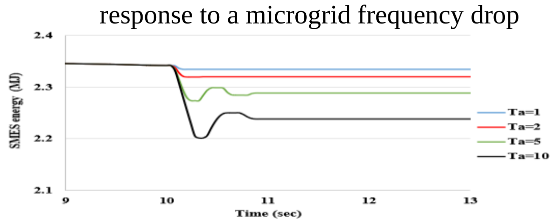

Fig. 18. SMES energy at different inertia constants in response to a microgrid frequency drop

To easily describe the effect of the inertia time constant on the converter power rating, the maximum converter output power values at each inertia time constant are traced with respect to the inertia time constants in Fig. 19. It is seen that the converter power increases when the inertia time constant increases. Moreover, the maximum SMES power and the supplied energy are sown in Fig. 20 and Fig. 21. It is shown that the SMES needs to supply more power and energy when the inertia time constant increases.

The next set of simulations describes the VSG operation when the reference power is changed. The reference power increased from 0.4 pu to 0.7 pu, and the system is simulated at different damping and inertia time constants. This change may be activated by the local controller or from a hierarchical control system in response to a load or generating power change.

Fig. 22 describes that the converter output power follows the reference values, however; the response depends on the damping constant. When the damping constant increases, the converter maximum output power decreases and it reaches the steady state sooner. The PV array generates 0.4 pu, and the converter output power increased from 0.4 pu to 0.7 pu. The difference is compensated by the HESS. The SMES has a fast response and handles the transient power oscillation. The SMES compensates for the oscillation of the converter output power due to its fast response. Then, it helps to reduce the stress on the battery and extends to increase its lifetime. The battery supplies the steady state power (0.3 pu). Fig. 23 describes the SMES supplied power and it shows that the SMES power increased when the damping constant decreased and it takes more time to reach its steady-state value. Fig. 24 describes how the virtual mechanical frequency changes. It is shown that when the damping constant increases, the frequency has a higher frequency nadir and the system is more stable against the system disturbance. Fig. (25) describes the battery discharge to compensate the steady state difference between the PV and load power.

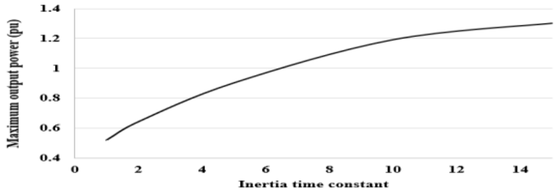

Fig. 19. Maximum output power versus inertia constants in response to a microgrid frequency drop

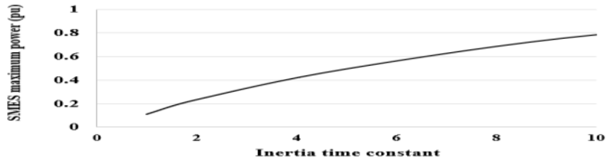

Fig. 20. SMES maximum power versus inertia constants in response to a microgrid frequency drop

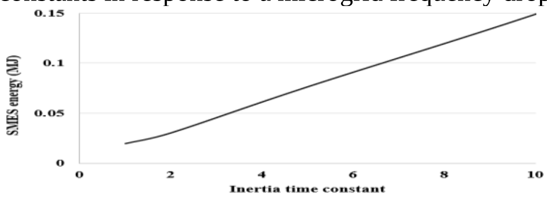

Fig. 21. SMES energy versus inertia constants in response to a microgrid frequency drop

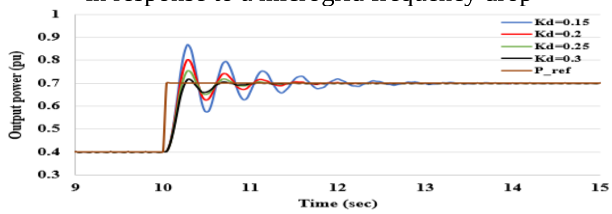

Fig. 22. Converter power at different damping constants in response to step power setpoint increase

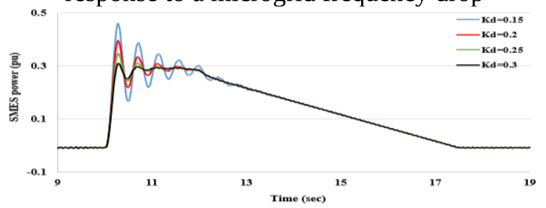

Fig. 23. SMES power at different damping constant in response to step power setpoint increase

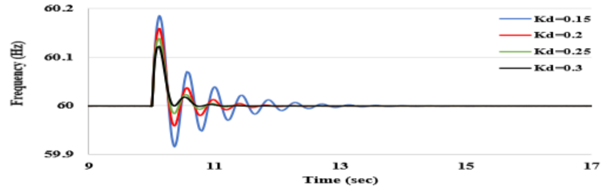

Fig. 24. Frequency change at different damping constants in response to step power setpoint increase

This test is repeated, the reference input power to the converter is increased at different inertia time constants. The converter output power profile is shown in Fig. 26, it is shown that the converter output power follows the reference power with a profile depending on the inertia time constant. At a smaller inertia time constant, the VSG supplies less inertial power, and it has a larger number of oscillations until it reaches its steady-state value.

The PV array generates 0.4 pu and the difference between the PV array power and the converter output power is compensated by the ESS. The SMES supplies the transient power and the battery supplies the steady state power. The SMES power is shown in Fig. 27. It is shown that at a smaller inertia time constant the SMES needs to supply less power. Then the rating power of the converter and the SMES system should be based on the emulated inertia time constants. Increasing the inertia helps the system to be more stable at different disturbances. As shown in Fig. 28, when the inertia time constant increases, the frequency has a smaller rate of change of the frequency (RoCoF) and a larger value of frequency nadir. Fig. (29) describes the battery discharge power, it supplies 0.3 pu.

To show the effect of both the inertia and damping constants on the system performance and the SMES power and energy rating, the system is simulated at different values of inertia and damping constants. Fig. 30 describes the converter maximum output power oscillation with respect to inertia time constant at different damping constants when the frequency change from 60 Hz to 59.5 Hz. It can be shown that the maximum value increases with increasing the inertia time constant and reduction in the damping constant.

Fig. 31 and Fig. 32 describe the SMES power and energy at different values of both inertia and damping constants. The SMES power and energy decrease with damping constant increase. Also, SMES power and energy are increased when the emulated inertia time constant increases.

It can be shown from the simulation results that the inertia time constant and the damping constant affects the system performance and sizing of both the converter and the SMES power and energy. Moreover, using the SMES ESS, the converter can emulate the inertial feature of a proposed CSG by adjusting the inertia and damping constants.

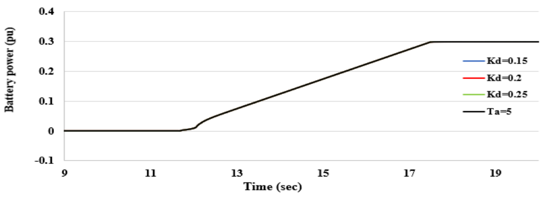

Fig. 25. Battery power profile

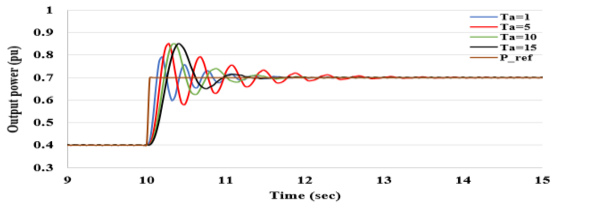

Fig. 26. Converter power at different inertia constants in response to step power setpoint increase

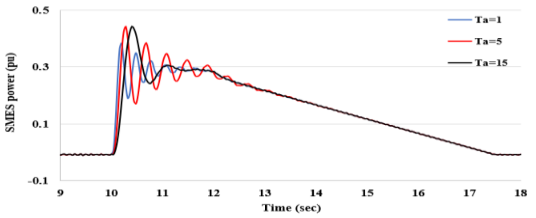

Fig. 27. SMES power at different inertia constants in response to step power setpoint increase

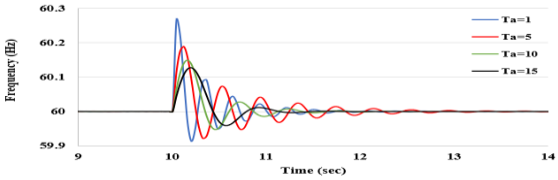

Fig. 28. Frequency change at different inertia constants in response to step power setpoint increase

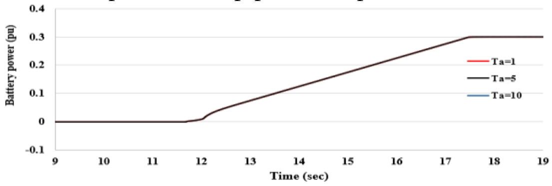

Fig. 29. Battery power profile

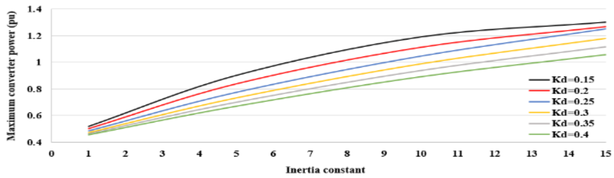

Fig. 30. Converter output power at different inertia and damping constants

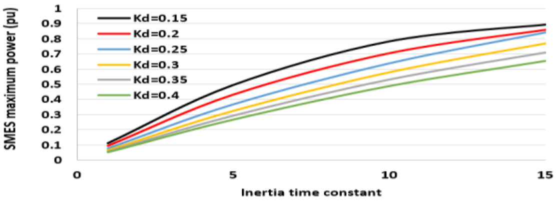

Fig. 31. SMES maximum power at different inertia and damping constants

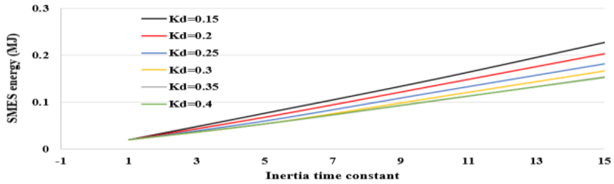

Fig. 32. SMES energy at different inertia and damping constants

7. CONCLUSION

The sudden changes in the load and generated power from RERs may cause fluctuations in the system and deteriorate the power quality. To counteract these changes, ESSs have been used to emulate the conventional synchronous generator inertia and damping constants, hence improving the system stability and operation against different disturbances.

In this paper, a hybrid energy storage system consists of a SMES system and a battery system is described. The system is implemented using an electromagnetic transients program. The system is simulated at different values of inertia time and damping constants. The impact of different values of constants affect the ratings of the converter and the SMES was described.

The converter output power and the SMES power and energy increases when the inertia time constant increases or the damping constant decreases. Also, VSG converter can emulate many CSG inertial features through changing the inertia and damping constants. Furthermore, VSG can enhance the system stability such as reducing the RoCoF or the frequency nadir through emulating the CSG inertial features. Supplementing the battery with the SMES reduces the number of charging and discharging cycles of the battery. Hence, this reduces the stress on the battery system and increases its lifetime.

VSG controllers combined with ESSs play a vital role to stabilize power system specially the small size systems such as microgrids and reshape the architecture of power networks. Also, this increases the ability of the system to support increasing penetration of RERs which helps to optimize using the available energy resources and minimize conventional fuel consumption and greenhouse gas emissions.

BIBLIOGRAPHY

[1] M. Haritha and D. S. Nair, “Review on virtual synchronous generator (VSG) for enhancing performance of microgrid,” in 2018 International Conference on Power, Signals, Control and Computation (EPSCICON)IEEE, 2018, pp. 1–5

[2] M. H. Othman, H. Mokhlis, M. Mubin, S. Talpur, N. F. Ab Aziz,M. Dradi, and H. Mohamad, “Progress in control and coordination ofenergy storage system-based VSG: A review,” IET Renewable Power Generation, vol. 14, no. 2, pp. 177–187, 2020.
[3] M. Abuagreb, B. Ajao, and B. K. Johnson, “Implementation of emulatedinertia using PV generation with energy storage to improve integratedgrid response,” in 2020 IEEE Texas Power and Energy Conference(TPEC). IEEE, 2020, pp. 1–6.
[4] J. Li, Q. Yang, F. Robinson, F. Liang, M. Zhang, and W. Yuan, “Designand test of a new droop control algorithm for a SMES/battery hybridenergy storage system,” Energy, vol. 118, pp. 1110–1122, 2017.
[5] M. Faisal, M. A. Hannan, P. J. Ker, A. Hussain, M. B. Mansor,and F. Blaabjerg, “Review of energy storage system technologies in microgrid applications: Issues and challenges,” IEEE Access, vol. 6, pp.35 143–35 164, 2018
[6] K. Divya and J. Ostergaard, “Battery energy storage technology for power systems— An overview,” Electric power systems research vol. 79, no. 4, pp. 511–520, 2009
[7] S. Hajiaghasi, A. Salemnia, and M. Hamzeh, “Hybrid energy storage system for microgrids applications: A review,” Journal of Energy Storage, vol. 21, pp. 543–570, 2019.
[8] A. Etxeberria, I. Vechiu, H. Camblong, and J.-M. Vinassa, “Hybrid energy storage systems for renewable energy sources integration in microgrids: A review,” in 2010 Conference Proceedings IPEC. IEEE,2010, pp. 532–537.
[9] T. Kerdphol, M. Watanabe, Y. Mitani, and V. Phunpeng, “Applying virtual inertia control topology to SMES system for frequency stability improvement of low-inertia microgrids driven by high renewables,” Energies, vol. 12, no. 20, p. 3902, 2019
[10] E. Saad, S. Helmy, Y. Elkoteshy, and U. AbouZayed, “Implementation of a modified MPPT strategy for solar-PV arrays connected to harmonic- polluted grids under partial shading conditions,” in 2021 International Telecommunications Conference (ITC-Egypt). IEEE, 2021, pp. 1–4.
[11] E. Saad, Y. Elkoteshy, and U. AbouZayed, “Modelling and analysis of grid-connected solar-PV system through current-mode controlled VSC,” in E3S Web of Conferences, vol. 167. EDP Sciences, 2020, p. 05005.
[12] M. Abuagreb, M. Allehyani, and B. K. Johnson, “Design and test of a combined PV and battery system under multiple load and irradiation conditions,” in 2019 IEEE Power & Energy Society Innovative Smart Grid Technologies Conference (ISGT). IEEE, 2019, pp. 1–5.
[13] M. M. Badreldien and B. K. Johnson, “Virtual synchronous generator controller for solar photovoltaic system,” in 2021 IEEE Electrical Power and Energy Conference (EPEC). IEEE, 2021, pp. 480–485.
[14] M. M. Badreldien, M. Abuagreb, M. F. Allehyani, and B. K. Johnson, “Modeling and control of solar PV system combined with battery energy storage system,” in 2021 IEEE Electrical Power and Energy Conference (EPEC). IEEE, 2021, pp. 373–377.
[15] S. D’Arco and J. A. Suul, “Virtual synchronous machines—classification of implementations and analysis of equivalence to droop controllers for microgrids,” in 2013 IEEE Grenoble Conference. IEEE, 2013, pp. 1–7.
[16] M. H. Ali, B. Wu, and R. A. Dougal, “An overview of SMES applications in power and energy systems,” IEEE transactions on sustainable energy, vol. 1, no. 1, pp. 38–47, 2010.
[17] M. Abuagreb, B. Ajao, H. Herbert, and B. K. Johnson, “Evaluation of virtual synchronous generator compared to synchronous generator,” in 2020 IEEE Power & Energy Society Innovative Smart Grid Technologies Conference (ISGT). IEEE, 2020, pp. 1–5.